Supplementary Material

This document contains:

- Texts S1 to S3
- Figures S1 to S12

Text S1 to S3

Text S1. Phase II – Paleoclimate conditions

During Phase II, the onset of drier and/or warmer conditions was inferred at ca. 17.8 ka BP (Moreno et al., 2018; Moreno and León, 2003), 17.6 ka BP (Montade et al., 2013) and 17 ka BP (Heusser et al., 2006b). The end of this drier phase was marked by a return to colder and/or wetter conditions at 14.8 ka BP (Moreno et al., 2018; Moreno and León, 2003), 14.7 ka BP (Haberle and Bennett, 2004), 14.6 ka BP (Pesce and Moreno, 2014), 14.5 ka BP(Montade et al., 2013; Moreno and Videla, 2016) and 14 ka BP (Heusser et al., 2006b; Jara and Moreno, 2014; Moreno, 2004; Moreno et al., 2010; Vargas-Ramirez et al., 2008). Note that the record of Murali et al 2010 suggests an onset of wetter conditions at 15.8 based on the composition of marine sediments (Figure S12). Here, we instead refer to the records of Heusser et al. (2006a) and Kaiser et al. (2024) that reconstructed past hydrological regime through the use of leaf-wax n-alkanes and pollens at the same site and implied a later return to wetter conditions.

Text S2. Phase III – Paleoclimate conditions

Phase III was marked by wet and cold conditions (see Text S1) followed by a transition period until ca. 11.5 ka BP – roughly corresponding to the Younger Dryas (ca. 12.9-11.6 ka BP). The onset of this transition period was dated at 13 ka BP (Moreno and Videla, 2016), 12.8 ka BP (Montade et al., 2013), 12.7 ka BP (Moreno et al., 2018; Pesce and Moreno, 2014), 12.4 ka BP (Jara and Moreno, 2014). In the record of Moreno (2004) and Moreno et al. (2010), we furthermore noted an increase in the ECPI index – a paleovegetation index reflecting past temperature and hydrological conditions at around 13 ka BP – indicating the onset of a transition to warmer and drier conditions. These reconstructions suggest a precipitation decrease and/or climate variability during the Younger Dryas.

Overall wet conditions were inferred until 12.3 ka BP (Haberle and Bennett, 2004), 12 ka BP (Heusser et al., 2006b), 11.6 ka BP (Abarzúa et al., 2004; Moreno and Videla, 2016; Vargas-Ramirez et al., 2008), 11.5 ka BP (Jara and Moreno, 2014; Montade et al., 2013; Moreno, 2004; Moreno et al., 2010), 11.3 ka BP (Moreno et al., 2018) and 11 ka BP (Moreno and León, 2003; Pesce and Moreno, 2014). Note that no transition period were detected in the records of Vargas-Ramirez et al. (2008), Heusser et al. (2006b), Moreno and León (2003), Haberle and Bennet (2004) and Abarzúa et al. (2004). These reconstructions are consistent with a colder and wetter period between ca. 14 and 12 ka BP and the onset of drier conditions at ca. 11.5 ka BP as suggested by the δ^2H_{wax} records of site GeoB3304-5 at 33°S.

Text S3 Phase IV – Paleoclimate conditions

Most records located between 40°S and 46°S indicated a transition from dry conditions to wet conditions between 8 and 7 ka BP. At 40°S, wetter conditions were detected at 8 ka BP by Vargas-Ramirez et al. (2008) and 7.1 ka BP (Jara and Moreno, 2014).In Vargas-Ramirez et al. (2008), these conditions were enhanced at 6.8 ka BP. Between 41°S and 44°S, wetter conditions were inferred after between 7.9 and 7.6 ka BP (Abarzúa et al., 2004; Moreno, 2004; Moreno et al., 2010, 2018; Moreno and León, 2003; Moreno and Videla, 2016; Pesce and Moreno, 2014). At 44°S, Haberle and Bennett (2004) suggested seasonally wet conditions between 6.8 and 2.7 ka BP.

Figures S1 to S13

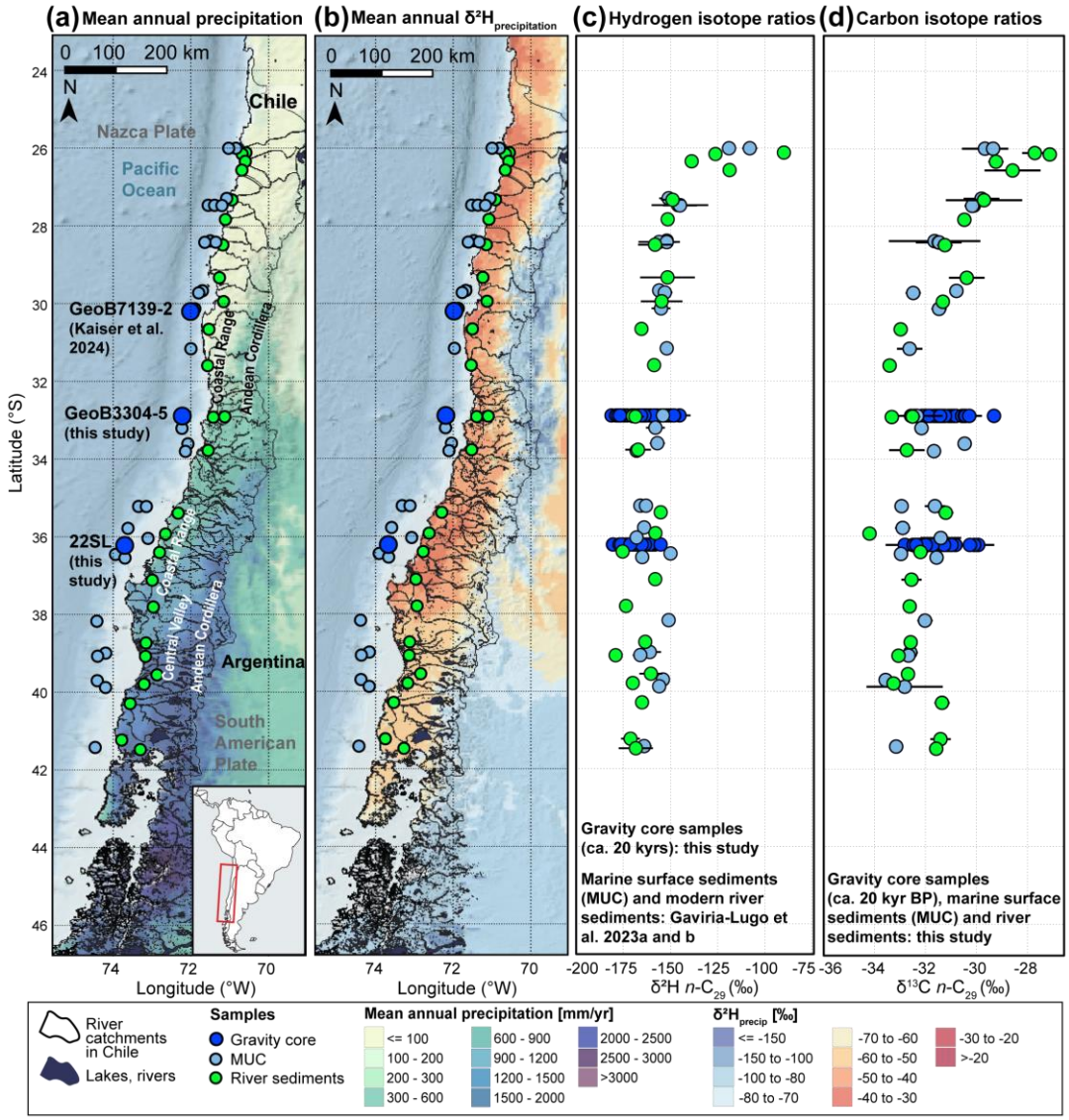

Figure S1. Sampling sites and the hydrogen and carbon isotope ratios (measured on *n*-C_{29} *n*-alkanes) of fluvial and marine sediments along Chile. Data represent present-day conditions (river and multicorer [MUC] sediments) and variability spanning ca. 20 kyr in gravity cores. (a) Mean annual precipitation map (TRMM 3B43, European Commission, Joint Research Centre (JRC), 2015) and sampling sites (this study, Gaviria-Lugo et al., 2023a; Kaiser et al., 2024). (b) Mean annual δ^2H_{precip} map (Bowen et al., 2005; Bowen and Revenaugh, 2003; Waterisotopes Database, 2017) and sampling sites (this study, Gaviria-Lugo et al., 2023a; Kaiser et al., 2024). (c) Hydrogen isotope composition (n-C_{29}) of modern fluvial sediments (green, Gaviria-Lugo et al., 2023a, b), marine surface sediments (MUC, light blue, Gaviria-Lugo et al., 2023a, b) and gravity cores (dark blue, site GeoB7139-2 from Kaiser et al., 2024 and sites GeoB3304-5 and 22SL) by latitude. (d) Carbon isotope composition (n-C_{29}) of fluvial sediments (green), marine surface sediments (light blue) and gravity cores (dark blue) by latitude (this study, see Gaviria-Lugo et al., 2023a for sample site description). The $\delta^{13}C$ ratio of modern river and MUC samples were corrected for the pre-industrial carbon isotope composition of the atmosphere (Section 3.4). Note the consistency of the modern hydrogen and carbon isotope ratios along Chile despite substantial changes in the mean annual precipitation amount (panel A). Digital Elevation Model is from the GEBCO Bathymetric Compilation Group (2019). The lake and river maps are from the Biblioteca del Congreso Nacional de Chile (accessed 31.03.2025). Watersheds are from Gaviria-Lugo et al. (2023a). Error bars in panels C and D correspond to two standard deviations (2σ) calculated from the δ^2H and the $\delta^{13}C$ values reported in Tables S5 to S7.

Figures S2-S7: Age models

The age models of the marine sites GeoB7139-2 (Figure S2 and S5), GeoB3304-5 (Figure S3 and S6), and 22SL (Figure S4 and S7) were generated using the R-Package rbacon v. 3.2.0 (Blaauw and Christen, 2011) for the scenarios 1 and 2.

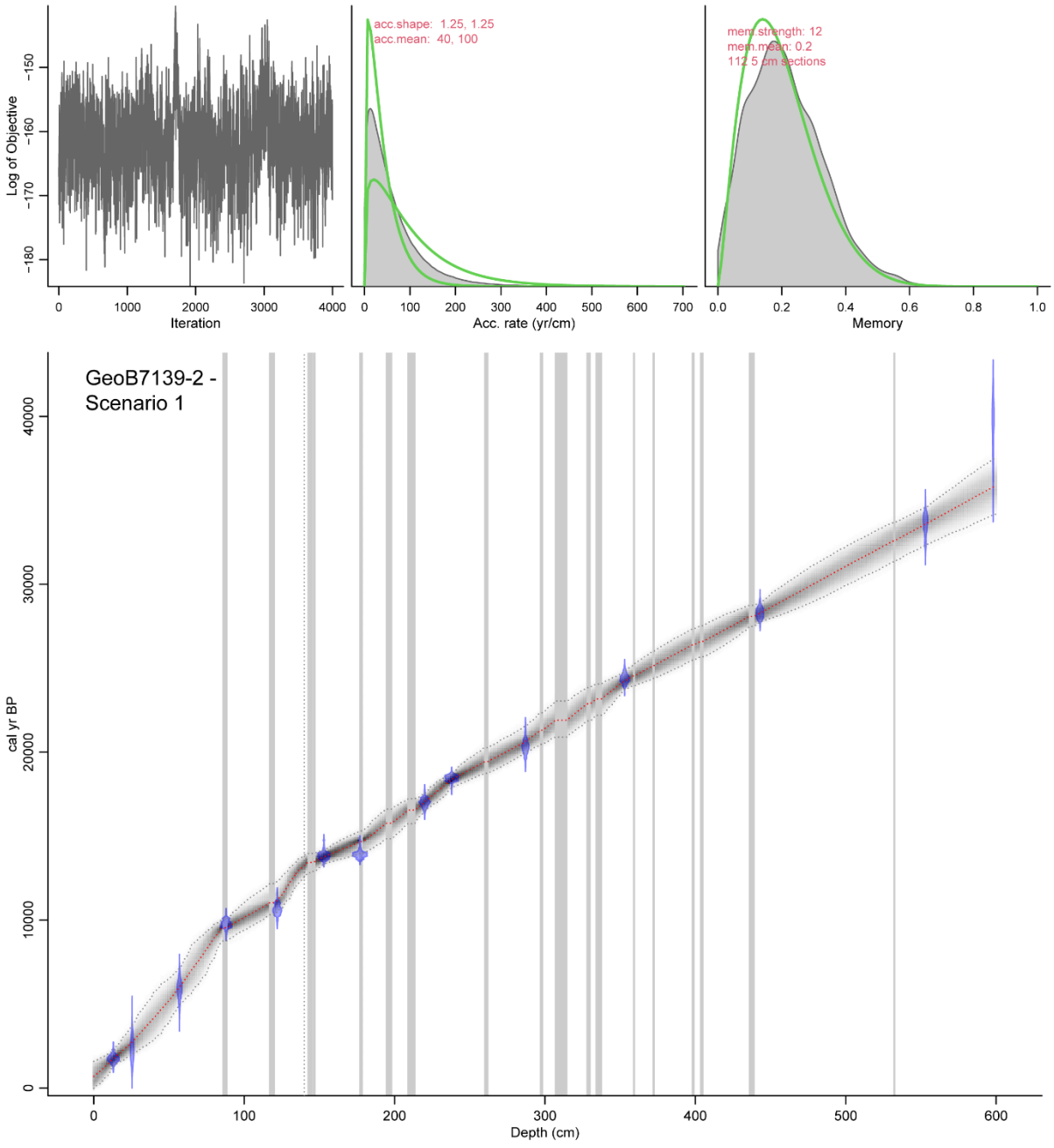

Figure S2. Age-depth model of the marine site GeoB7139-2 (Scenario 1) reconstructed and plotted using the rbacon R Package (Blaauw and Christen, 2011)**.** A boundary was defined at 140 cm. The settings used were acc.mean=100 between 0 and 140 cm, acc.mean=40 between 140 and 600 cm, acc.shape=1.25, mem.strength=12 and mem.mean=0.2. The calibrated radiocarbon ages and their uncertainties were displayed in blue. The red and grey dashed curve corresponded to the mean and 95% confidence interval of the age-depth model, respectively. Turbidites layers were indicated by grey rectangles.

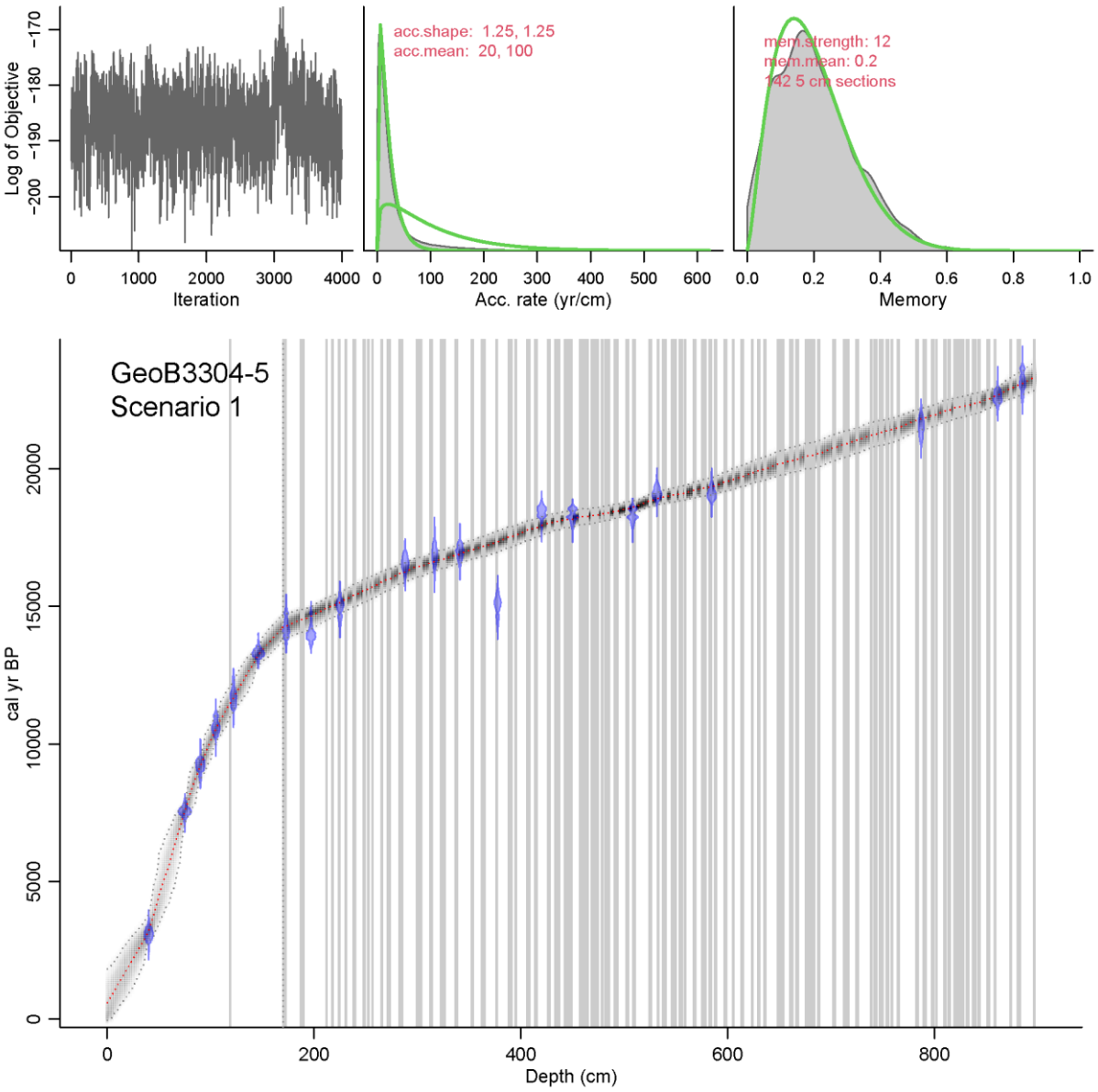

Figure S3. Age-depth model of the marine site GeoB3304-5 (Scenario 1) reconstructed and plotted using the rbacon R Package (Blaauw and Christen, 2011)**.** A boundary was defined at 170 cm. The settings used were acc.mean=100 between 0 and 170 cm, acc.mean=20 between 170 and 897 cm, acc.shape=1.25, mem.strength=12, and mem.mean=0.2. See Figure S2 for the legend.

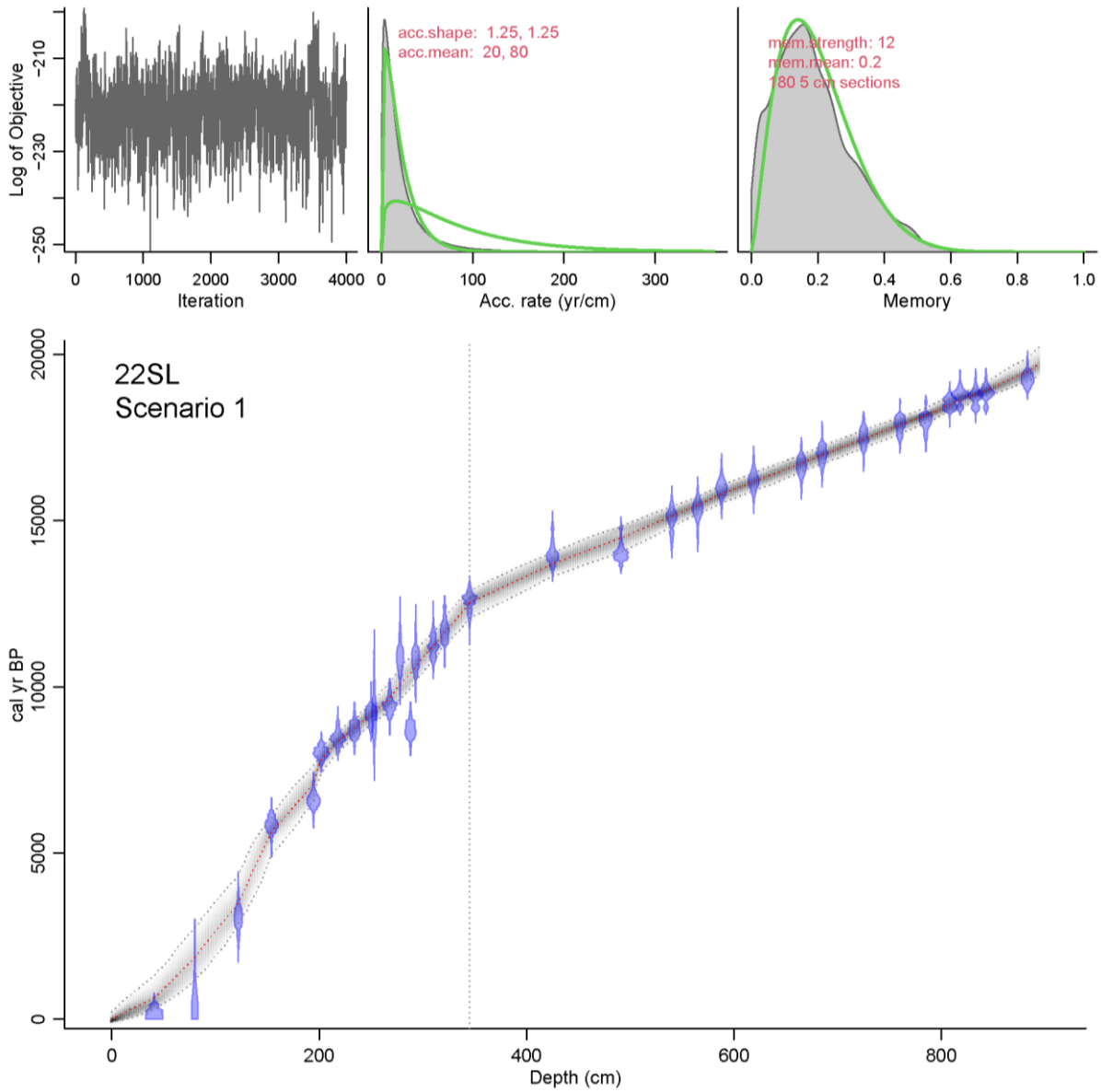

Figure S4. Age-depth model of the marine site 22SL (Scenario 1) reconstructed and plotted using the rbacon R Package (Blaauw and Christen, 2011)**.** A boundary (dashed line) was defined at 345 cm. The settings used were acc.mean=80 between 0 and 345 cm, acc.mean=20 between 345and 894 cm, acc.shape=1.25, mem.strength=12 and mem.mean=0.2. See Figure S2 for the legend.

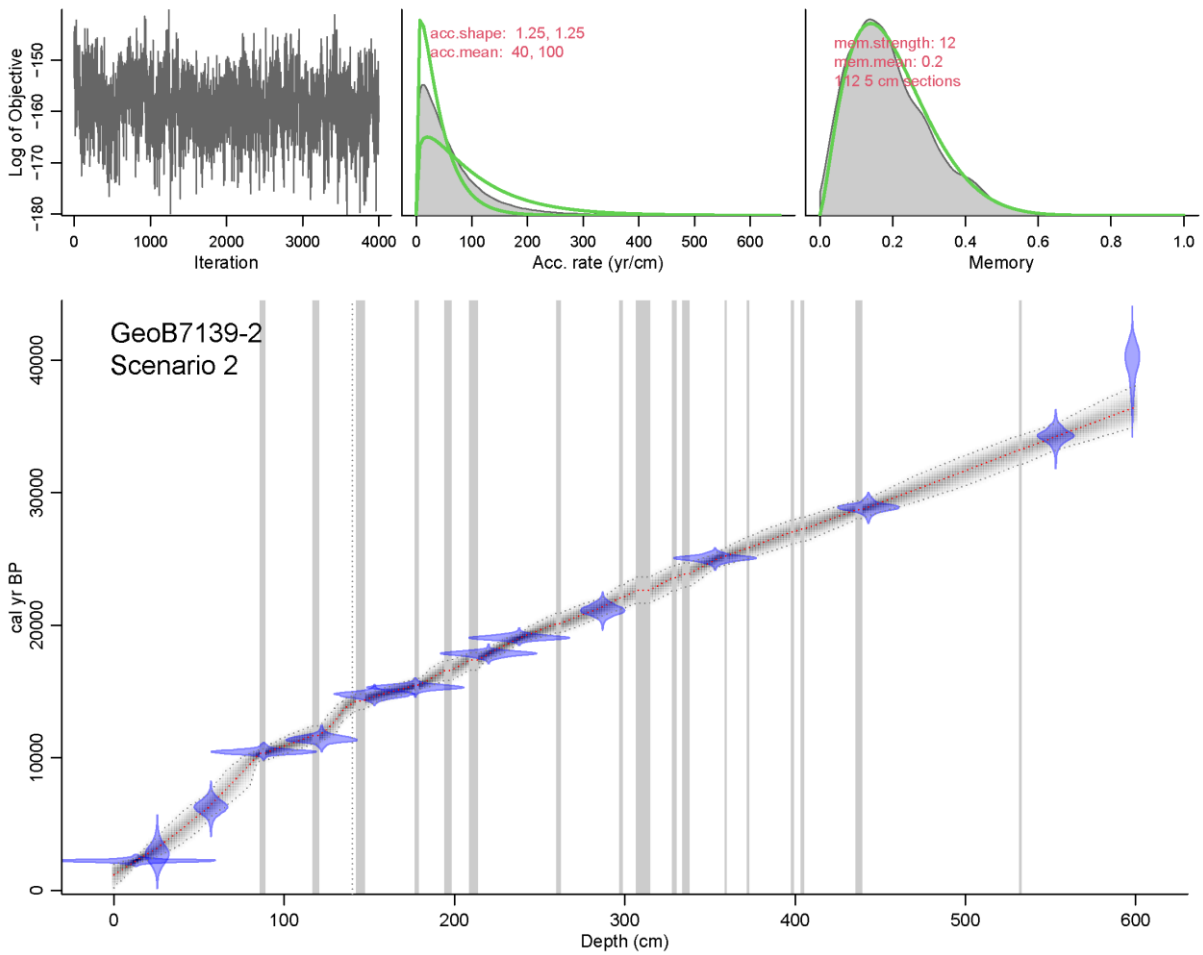

Figure S5. Age-depth model of the marine site GeoB7139-2 (Scenario 2) reconstructed and plotted using the rbacon R Package (Blaauw and Christen, 2011)**.** A boundary was defined at 140 cm. The settings used were acc.mean=100 between 0 and 140 cm, acc.mean=40 between 140 and 600 cm, acc.shape=1.25, mem.strength=12 and mem.mean=0.2. The calibrated radiocarbon ages and their uncertainties were displayed in blue. The red and grey dashed curve corresponded to the mean and 95% confidence interval of the age-depth model, respectively. Turbidites layers were indicated by grey rectangles.

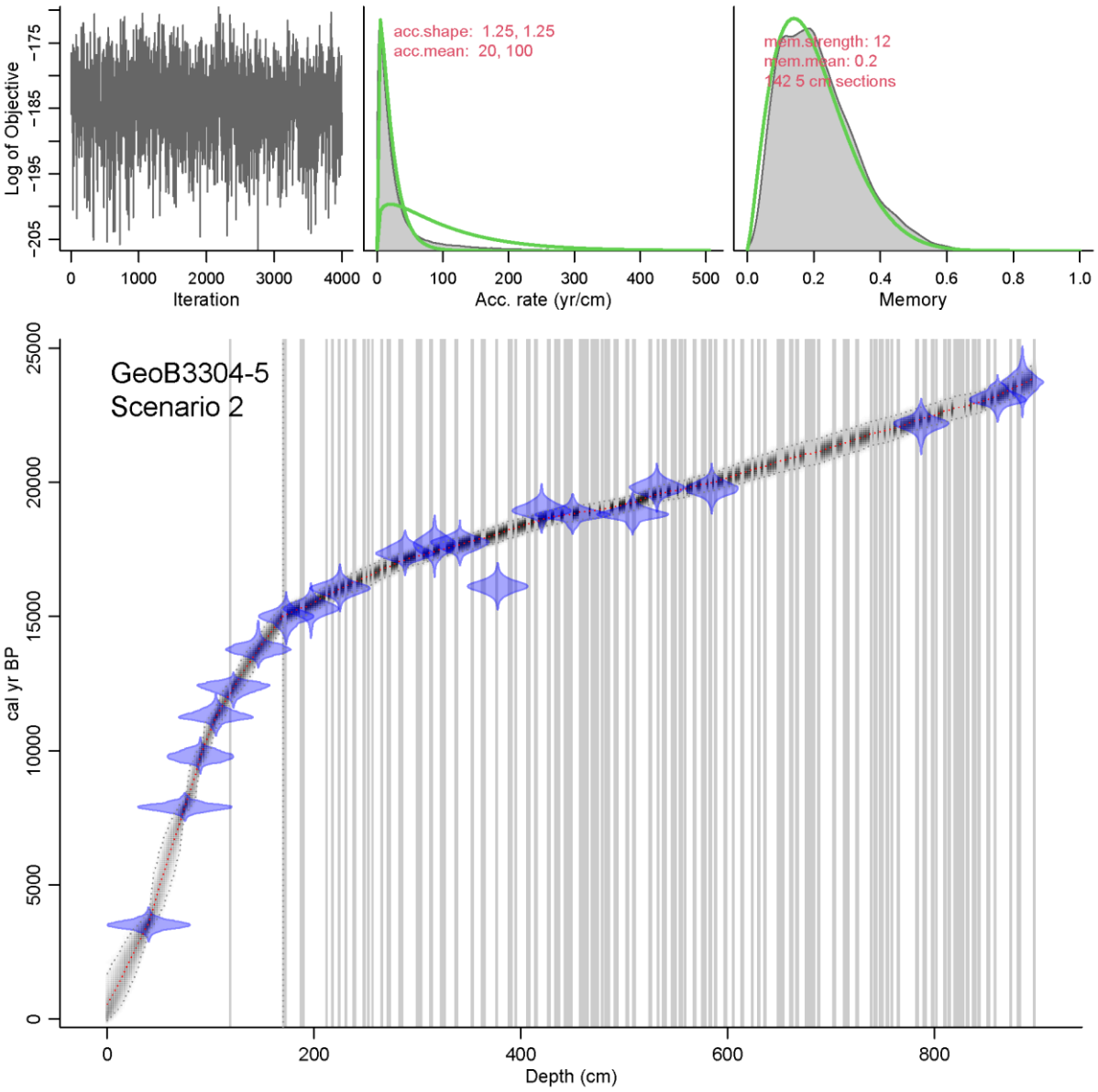

Figure S6. Age-depth model of the marine site GeoB3304-5 (Scenario 2) reconstructed and plotted using the rbacon R Package (Blaauw and Christen, 2011)**.** A boundary was defined at 170 cm. The settings used were acc.mean=100 between 0 and 170 cm, acc.mean=20 between 170 and 897 cm, acc.shape=1.25, mem.strength=12, and mem.mean=0.2. See Figure S5 for the legend.

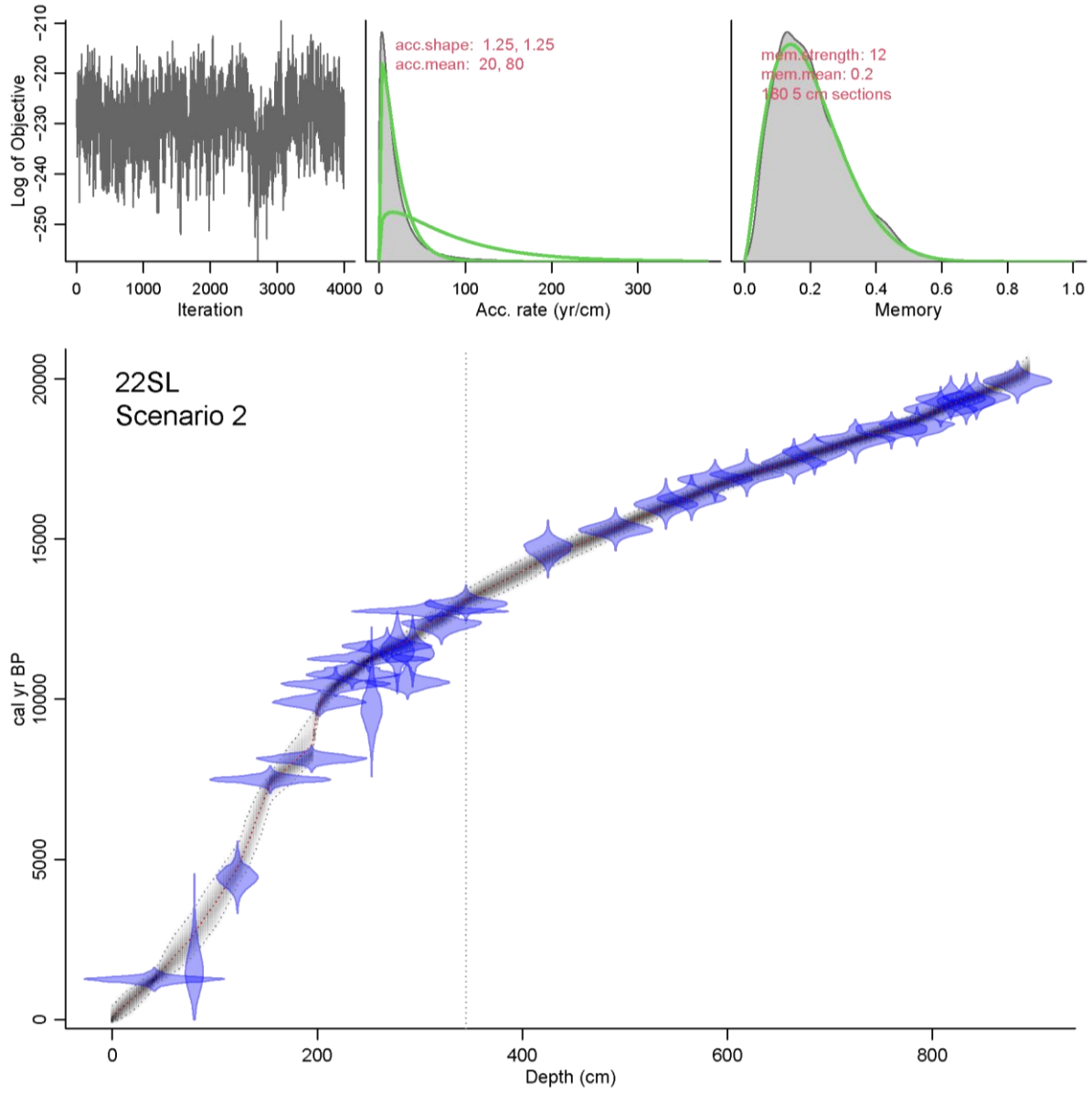

Figure S7. Age-depth model of the marine site 22SL (Scenario 2) reconstructed and plotted using the rbacon R Package (Blaauw and Christen, 2011)**.** A boundary (dashed line) was defined at 345 cm. The settings used were acc.mean=80 between 0 and 345 cm, acc.mean=20 between 345and 894 cm, acc.shape=1.25, mem.strength=12 and mem.mean=0.2. See Figure S5 for the legend.

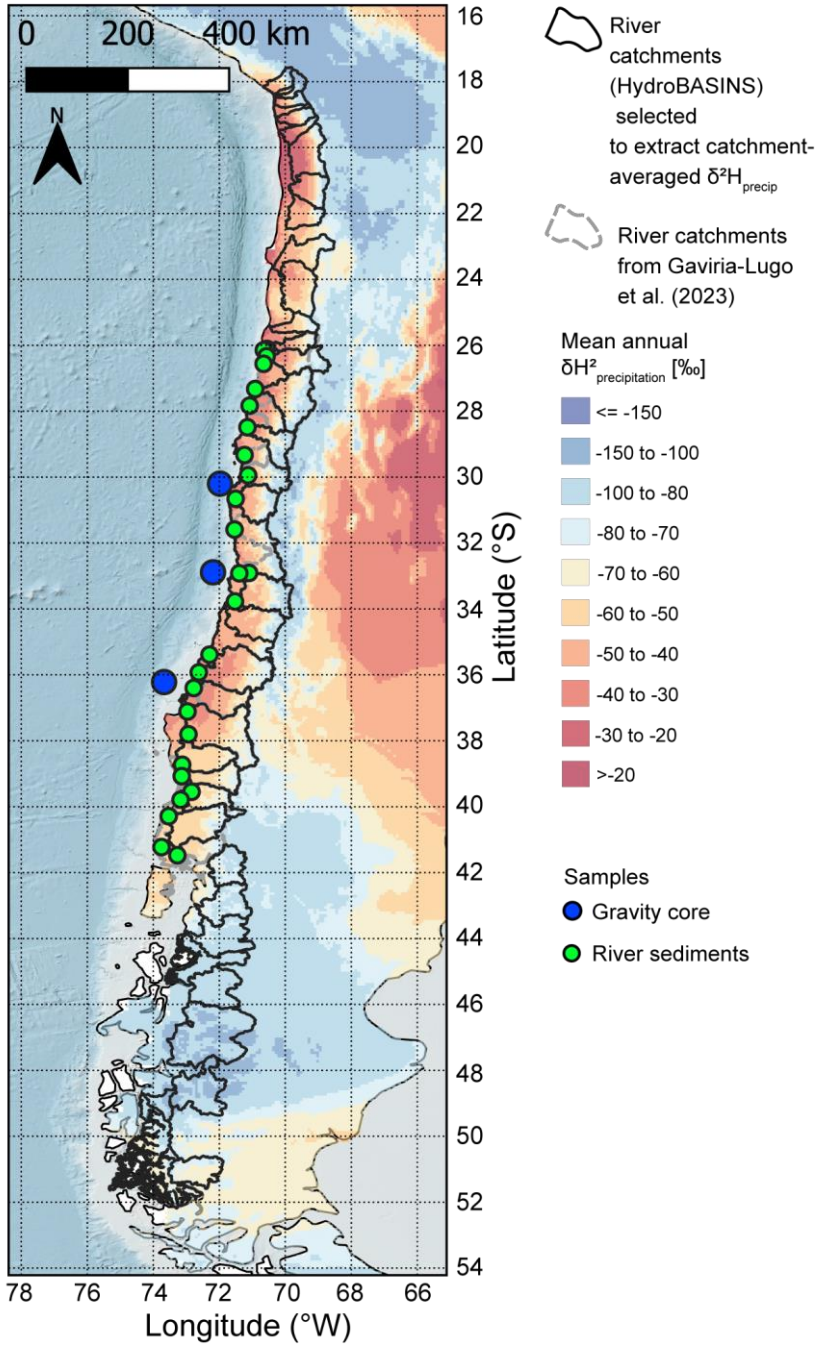

Figure S8. Catchment contours of the HydroBASINS Level 6 map (Hydroshed, Lehner et al., 2006; Lehner and Grill, 2013) compared with the catchment contours from Gaviria-Lugo et al. (2023a) with sampling sites. Fluvial sediments (green), and gravity cores (dark blue). Mean annual δ^2H_{precip} map (Bowen et al., 2005; Bowen and Revenaugh, 2003; Waterisotopes Database, 2017). HydroBASINS map accessed the 27.03.2025.

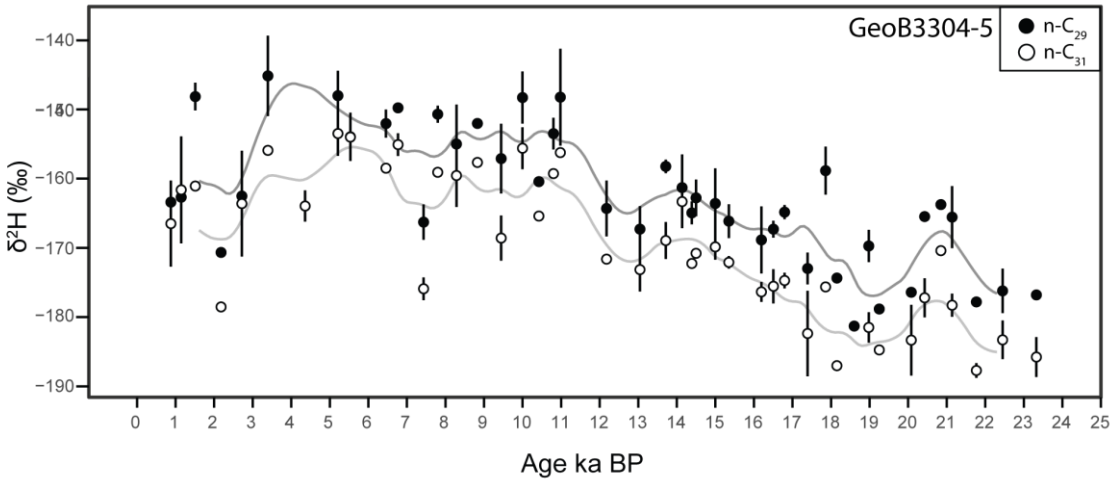

Figure S9. Hydrogen isotope records (δ^2H_{wax}) of the *n*-alkane homologues *n*-C_{29} and *n*-C_{31} of site GeoB3304-5. Note the similarities in the trends of the two homologues during the last 20 kyr, except at about 4 ka BP. The two standard deviations (2σ) calculated from the values reported in the Tables S5 and S6 were indicated for the δ^2H (*n*-C_{29}) values.

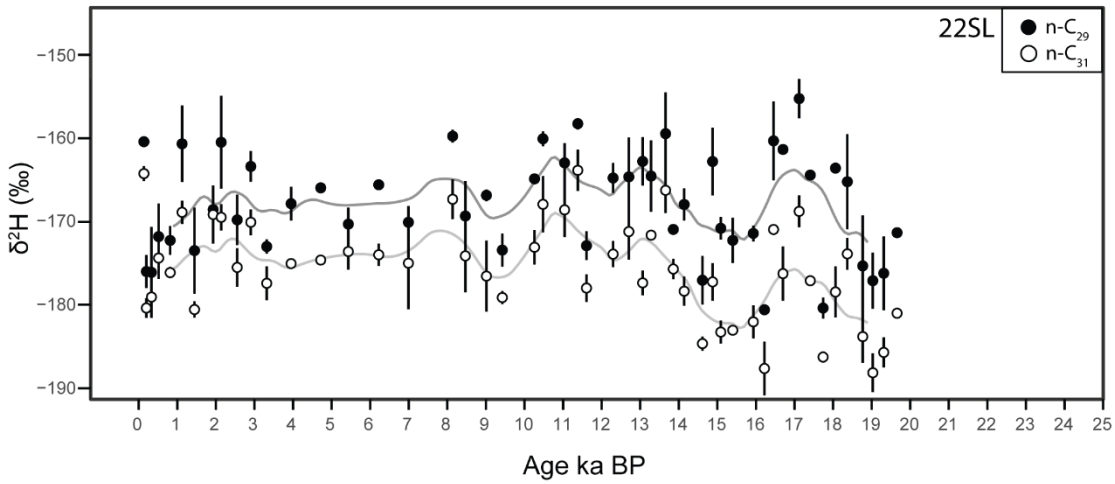

Figure S10. Hydrogen isotope records (δ^2H_{wax}) of the *n*-alkane homologues *n*-C_{29} and *n*-C_{31} of site 22SL. Note the similarities in the trends of the two homologues during the last 20 kyr. The two standard deviations (2σ) calculated from the values reported in the Tables S5 and S6 were indicated for the δ^2H (*n*-C_{29}) values.

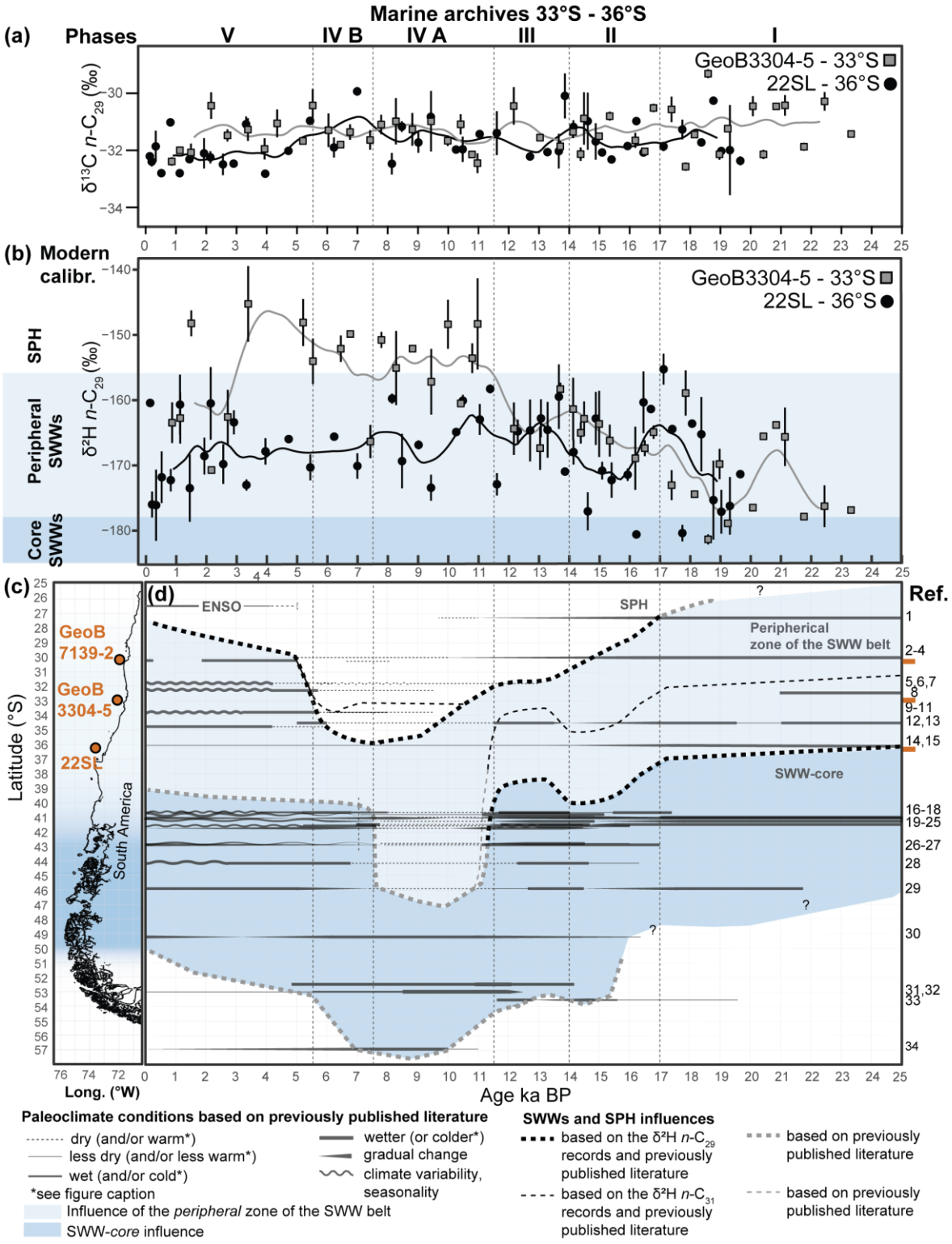

Figure S11. Reconstruction of the past extent of the SWW belt and the SPH based on the hydrogen isotope records of leaf-wax *n*-alkanes (*n*-C$_{29}$) and previously published literature. (a) δ^2H_{wax} records of sites GeoB7139-2 (30°S, Kaiser et al., 2024), GeoB3304-5 and 22SL. (b) $\delta^{13}C_{wax}$ records of sites GeoB3304-5 and 22SL. (c) Map of the west coast of South America between the latitudes of 25°S and 56°S with the locations of the marine sites. (d) Reconstruction of the past extend of the SWW belt and the SPH. Note the southward migration of the SWW belt at around 17 ka BP, its northward migration during Phase III, its abrupt shift southward during Phase IV and its return northward during Phase V. References: (1) (Stuut and Lamy, 2004), (2) (Muñoz et al., 2020), (3) (Kaiser et al., 2008), (4) (Bernhardt et al., 2017), (5) (Ortega et al., 2012), (6) (Maldonado and Villagrán, 2002), (7) (Maldonado and Villagrán, 2006), (8) (Flores-Aqueveque et al., 2021), (9) (Jenny et al., 2002), (10)

(Jenny et al., 2003), (11) (Villa-Martínez et al., 2003), (12) (Valero-Garcés et al., 2005), (13) (Frugone-Álvarez et al., 2017), (14) (Heusser et al., 2006a), (15) (Muratli et al., 2010), (16) (Vargas-Ramirez et al., 2008) in which only a cooling was recorded during the ACR, (17) (Jara and Moreno, 2014), (18) (Jara and Moreno, 2012), (19) (Heusser et al., 2006b), (20) (Kaiser et al., 2024), (21) (Moreno et al., 2018), (22) (Moreno and León, 2003), in which only a cooling was recorded during the ACR (23) (Moreno and Videla, 2016), (24) (Moreno, 2004), (25) (Moreno et al., 2010), (26) (Pesce and Moreno, 2014), (27) (Abarzúa et al., 2004), (28) (Haberle and Bennett, 2004), (29) (Montade et al., 2013), (30) (Ashworth et al., 1991), (31) (Fesq-Martin et al., 2004), (32) (Lamy et al., 2010), centered at 53°S, (33) (Heusser et al., 2000), and (34) (Perren et al., 2025). See Sections 5.3.1 to 5.3.5; Text S1 to S3 and Figure S12 for details. Error bars correspond to two standard deviations (2σ) calculated from the values reported in the Tables S5 and S6. The gradient of blue shades in panel C schematically reflects the *core* and *peripheral* zone of the SWW belt as shown in Figure 3.

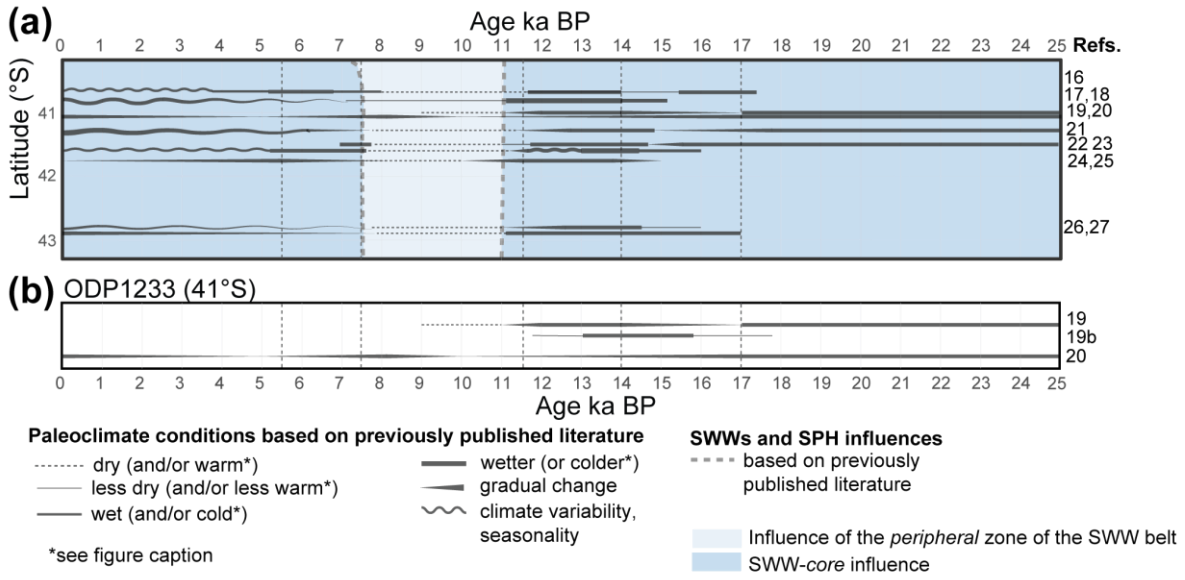

Figure S12. Reconstruction of the past extend of the SWWs based on previously published literature between ca. 40°S and 43°S. (a) Reconstruction of the past extend of the SWWs between 40°S and 43°S with relative changes in humidity and/or temperature. (b) Comparison of relative changes in humidity previously inferred at site ODP 1233 (41°S). References from Figure 4 and S11: (16) (Vargas-Ramirez et al., 2008) note that only a cooling was recorded during the ACR, (17) (Jara and Moreno, 2014), (18) (Jara and Moreno, 2012), (19) (Heusser et al., 2006b), (19b) (Muratli et al., 2010), (20) (Kaiser et al., 2024), (21) (Moreno et al., 2018), (22) (Moreno and León, 2003), note that only a cooling was recorded during the ACR (23) (Moreno and Videla, 2016), (24) (Moreno, 2004), (25) (Moreno et al., 2010), (26) (Pesce and Moreno, 2014), (27) (Abarzúa et al., 2004).

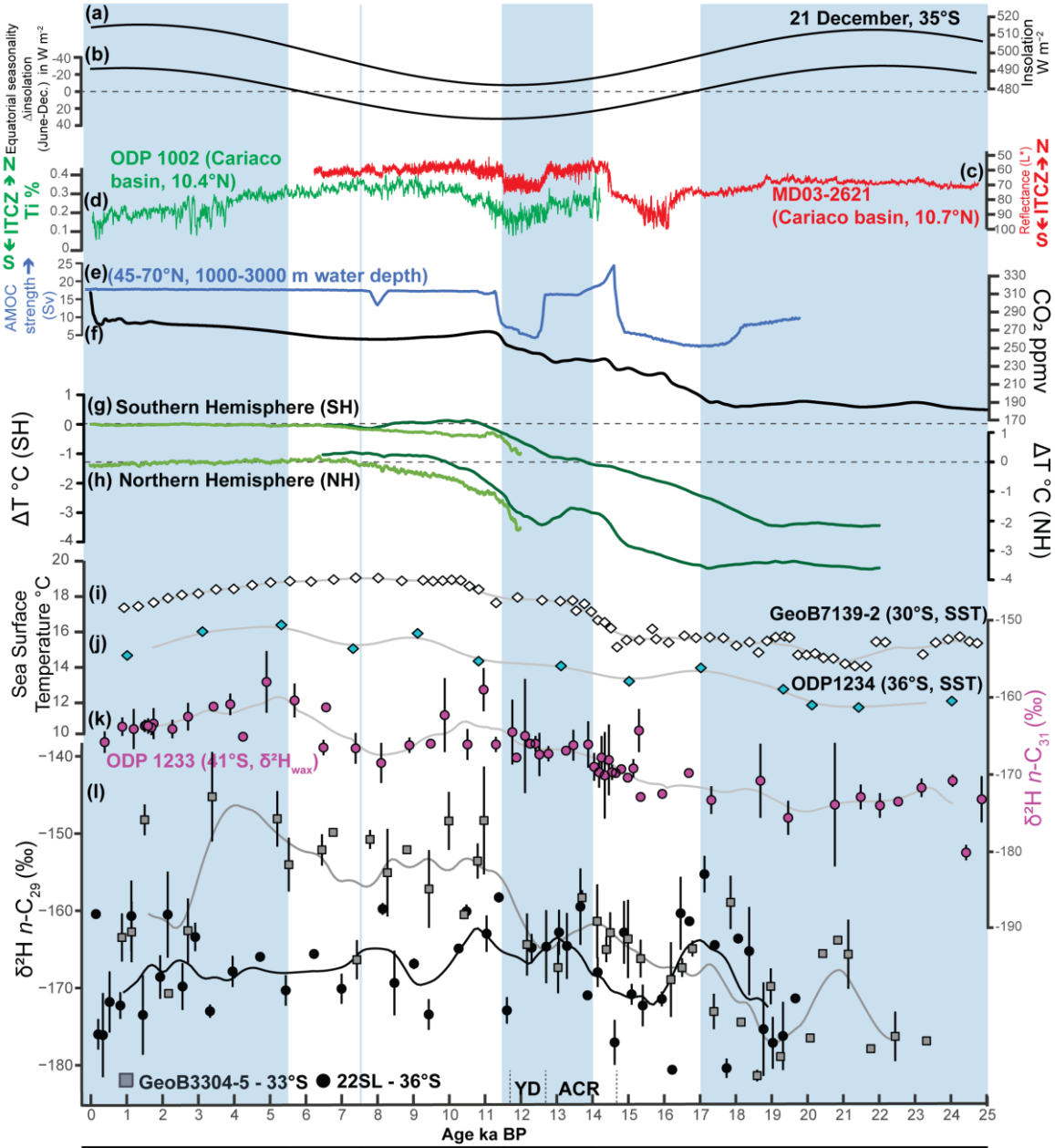

Phase	V	IVB	IVA	III-ACR / III-YD	II	I
Age	5 kyr BP - Present	7 - 5 kyr BP	11.5 - 7 kyr BP	14 - 11.5 kyr BP	17 - 14 kyr BP	>17 kyr BP
ITCZ	migration South	North	North	North / South	migr. further South	South of modern position
SWW	migration North	North	South	? / North	migr. further South	North of modern position
Atm. path.	ENSO (El-Niño)	?	ENSO (La-Niña)	ΔT hemisph.	ΔT hemisph.	?

Figure S13. Comparison of the leaf-wax *n*-alkane hydrogen isotope records (*n*-C$_{29}$, l) to past changes in insolation (a), seasonality (b) and independent paleoenvironmental records (c-k). (a) Equatorial seasonality modelled as the difference in insolation between June and December at the equator (Berger, 1988; Berger and Loutre, 1991). (b) Past insolation during the austral summer at the latitude of 35°S (Berger, 1988; Berger and Loutre, 1991). (c) Reflectance at site MD03-2621 indicating past latitudinal migrations of the ITCZ (Deplazes et al., 2013). (d) Titanium content of site ODP 1002 indicating past latitudinal migrations of the ITCZ (Haug et al., 2001). (e) AMOC strength derived from the model of Pöppelmeier et al. (2023) for the North Atlantic (45-70°N) between 1000 and 3000 m water depth. (f) Continuous record of atmospheric CO_2 (spline-smoothed data) compiled

by Köhler et al. (2017a, b). (g) Southern Hemisphere surface temperature from Shakun et al. (2012, dark green) and Erb et al. (2022, light green) reported as temperature difference to pre-industrial values (ΔT). (h) Northern Hemisphere surface temperature from Shakun et al. (2012, dark green) and Erb et al. (2022, light green) reported as temperature difference to pre-industrial values (ΔT). (i) Sea surface temperature ($U^{k'}_{37}$, SST) at site GeoB7139-2 (30°S, Kaiser et al., 2008, 2024). (j) Sea surface temperature ($U^{k'}_{37}$, SST) at site ODP 1234 (36°S, de Bar et al., 2018a, b). (k) δ^2H_{wax} (*n*-C_{31}) record of site ODP 1233 (41°S, Kaiser et al., 2024). (l) δ^2H_{wax} (*n*-C_{29}) record of sites GeoB7139-2 (30°S, Kaiser et al., 2024), GeoB3304-5 (33°S) and 22SL (36°S). Error bars in (l) represent two standard deviations (2σ) calculated from the values reported in Tables S5 and S6.

References

Abarzúa, A. M., Villagrán, C., and Moreno, P. I.: Deglacial and postglacial climate history in east-central Isla Grande De Chiloé, Southern Chile (43°S), Quat. Res., 62, 49–59, https://doi.org/10.1016/j.yqres.2004.04.005, 2004.

Ashworth, A. C., Markgraf, V., and Villagran, C.: Late Quaternary climatic history of the Chilean Channels based on fossil pollen and beetle analyses, with an analysis of the modern vegetation and pollen rain, J. Quat. Sci., 6, 279–291, https://doi.org/10.1002/jqs.3390060403, 1991.

de Bar, M. W., Stolwijk, D. J., McManus, J. F., Sinninghe Damsté, J. S., and Schouten, S.: A Late Quaternary climate record based on long-chain diol proxies from the Chilean margin, Clim. Past, 14, 1783–1803, https://doi.org/10.5194/cp-14-1783-2018, 2018a.

de Bar, M. W., Stolwijk, D., McManus, J. F., Sinninghe Damsté, J. S., and Schouten, S.: Organic geochemistry of ODP Site 202-1234, https://doi.org/10.1594/PANGAEA.892651, 2018b.

Berger, A.: Milankovitch Theory and climate, Rev. Geophys., 26, 624–657, https://doi.org/10.1029/RG026i004p00624, 1988.

Berger, A. and Loutre, M. F.: Insolation values for the climate of the last 10 million years, Quat. Sci. Rev., 10, 297–317, https://doi.org/10.1016/0277-3791(91)90033-Q, 1991.

Bernhardt, A., Schwanghart, W., Hebbeln, D., Stuut, J.-B. W., and Strecker, M. R.: Immediate propagation of deglacial environmental change to deep-marine turbidite systems along the Chile convergent margin, Earth Planet. Sci. Lett., 473, 190–204, https://doi.org/10.1016/j.epsl.2017.05.017, 2017.

Blaauw, M. and Christen, J. A.: Flexible paleoclimate age-depth models using an autoregressive gamma process, Bayesian Anal., 6, 457–474, https://doi.org/10.1214/11-BA618, 2011.

Bowen, G. J. and Revenaugh, J.: Interpolating the isotopic composition of modern meteoric precipitation, Water Resour. Res., 39, https://doi.org/10.1029/2003WR002086, 2003.

Bowen, G. J., Wassenaar, L. I., and Hobson, K. A.: Global application of stable hydrogen and oxygen isotopes to wildlife forensics, Oecologia, 143, 337–348, https://doi.org/10.1007/s00442-004-1813-y, 2005.

Deplazes, G., Lückge, A., Peterson, L. C., Timmermann, A., Hamann, Y., Hughen, K. A., Röhl, U., Laj, C., Cane, M. A., Sigman, D. M., and Haug, G. H.: Links between tropical rainfall and North Atlantic climate during the last glacial period, Nat. Geosci., 6, 213–217, https://doi.org/10.1038/ngeo1712, 2013.

Erb, M. P., McKay, N. P., Steiger, N., Dee, S., Hancock, C., Ivanovic, R. F., Gregoire, L. J., and Valdes, P.: Reconstructing Holocene temperatures in time and space using paleoclimate data assimilation, Clim. Past, 18, 2599–2629, https://doi.org/10.5194/cp-18-2599-2022, 2022.

European Commission, Joint Research Centre (JRC): South America Mean Annual Precipitation Map (TRMM 3B43 dataset), 2015.

Fesq-Martin, M., Friedmann, A., Peters, M., Behrmann, J., and Kilian, R.: Late-glacial and Holocene vegetation history of the Magellanic rain forest in southwestern Patagonia, Chile, Veg. Hist. Archaeobotany, 13, 249–255, https://doi.org/10.1007/s00334-004-0047-6, 2004.

Flores-Aqueveque, V., Ortega, C., Fernández, R., Carabias, D., Simonetti, R., Cartajena, I., Díaz, L., and González, C.: A multi-proxy reconstruction of depositional environment of a Late Pleistocene submerged site from the Central Coast of Chile (32°): Implications for drowned sites, Quat. Int., 601, 15–27, https://doi.org/10.1016/j.quaint.2021.06.005, 2021.

Frugone-Álvarez, M., Latorre, C., Giralt, S., Polanco-Martínez, J., Bernárdez, P., Oliva-Urcia, B., Maldonado, A., Carrevedo, M. L., Moreno, A., Delgado Huertas, A., Prego, R., Barreiro-Lostres, F., and Valero-Garcés, B.: A 7000-year high-resolution lake sediment record from coastal central Chile (Lago Vichuquén, 34°S): implications for past sea level and environmental variability, J. Quat. Sci., 32, 830–844, https://doi.org/10.1002/jqs.2936, 2017.

Gaviria-Lugo, N., Läuchli, C., Wittmann, H., Bernhard, A., Frings, P., Mohtadi, M., Rach, O., and Sachse, D.: Climatic controls on leaf wax hydrogen isotope ratios in terrestrial and marine sediments along a hyperarid to humid gradient, EGUsphere, 1–34, https://doi.org/10.5194/egusphere-2023-831, 2023a.

Gaviria-Lugo, N., Läuchli, C., Wittmann, H., Bernhard, A., Frings, P., Mohtadi, M., Rach, O., and Sachse, D.: Data of leaf wax hydrogen isotope ratios and climatic variables along an aridity gradient in Chile and globally, https://doi.org/10.5880/GFZ.3.3.2023.001, 2023b.

Group, G. B. C.: The GEBCO_2019 grid—A continuous terrain model of the global oceans and land, Liverp. UK Br. Oceanogr. Data Cent. Natl. Oceanogr. Cent. NERC, 2019.

Haberle, S. G. and Bennett, K. D.: Postglacial formation and dynamics of North Patagonian Rainforest in the Chonos Archipelago, Southern Chile, Quat. Sci. Rev., 23, 2433–2452, https://doi.org/10.1016/j.quascirev.2004.03.001, 2004.

Haug, G. H., Hughen, K. A., Sigman, D. M., Peterson, L. C., and Röhl, U.: Southward Migration of the Intertropical Convergence Zone Through the Holocene, Science, 293, 1304–1308, https://doi.org/10.1126/science.1059725, 2001.

Heusser, C. J., Heusser, L. E., Lowell, T. V., M., A. M., and M., S. M.: Deglacial palaeoclimate at Puerto del Hambre, subantarctic Patagonia, Chile, J. Quat. Sci., 15, 101–114, https://doi.org/10.1002/(SICI)1099-1417(200002)15:2<101::AID-JQS500>3.0.CO;2-Y, 2000.

Heusser, L. E., Heusser, C. J., Mix, A., and McManus, J.: Chilean and Southeast Pacific paleoclimate variations during the last glacial cycle: directly correlated pollen and δ18O records from ODP Site 1234, Quat. Sci. Rev., 25, 3404–3415, https://doi.org/10.1016/j.quascirev.2006.03.011, 2006a.

Heusser, L. E., Heusser, C. J., and Pisias, N.: Vegetation and climate dynamics of southern Chile during the past 50,000 years: results of ODP Site 1233 pollen analysis, Quat. Sci. Rev., 25, 474–485, https://doi.org/10.1016/j.quascirev.2005.04.009, 2006b.

Jara, I. A. and Moreno, P. I.: Temperate rainforest response to climate change and disturbance agents in northwestern Patagonia (41°S) over the last 2600 years, Quat. Res., 77, 235–244, https://doi.org/10.1016/j.yqres.2011.11.011, 2012.

Jara, I. A. and Moreno, P. I.: Climatic and disturbance influences on the temperate rainforests of northwestern Patagonia (40 °S) since ∼14,500 cal yr BP, Quat. Sci. Rev., 90, 217–228, https://doi.org/10.1016/j.quascirev.2014.01.024, 2014.

Jenny, B., Valero-Garcés, B. L., Villa-Martínez, R., Urrutia, R., Geyh, M., and Veit, H.: Early to Mid-Holocene Aridity in Central Chile and the Southern Westerlies: The Laguna Aculeo Record (34°S), Quat. Res., 58, 160–170, https://doi.org/10.1006/qres.2002.2370, 2002.

Jenny, B., Wilhelm, D., and Valero-Garcés, B.: The Southern Westerlies in Central Chile: Holocene precipitation estimates based on a water balance model for Laguna Aculeo (33°50'S), Clim. Dyn., 20, 269–280, https://doi.org/10.1007/s00382-002-0267-3, 2003.

Kaiser, J., Schefuß, E., Lamy, F., Mohtadi, M., and Hebbeln, D.: Glacial to Holocene changes in sea surface temperature and coastal vegetation in north central Chile: high versus low latitude forcing, Quat. Sci. Rev., 27, 2064–2075, https://doi.org/10.1016/j.quascirev.2008.08.025, 2008.

Kaiser, J., Schefuß, E., Collins, J., Garreaud, R., Stuut, J.-B. W., Ruggieri, N., De Pol-Holz, R., and Lamy, F.: Orbital modulation of subtropical versus subantarctic moisture sources in the southeast Pacific mid-latitudes, Nat. Commun., 15, 7512, https://doi.org/10.1038/s41467-024-51985-4, 2024.

Köhler, P., Nehrbass-Ahles, C., Schmitt, J., Stocker, T. F., and Fischer, H.: A 156 kyr smoothed history of the atmospheric greenhouse gases CO_2, CH_4, and N_2O and their radiative forcing, Earth Syst. Sci. Data, 9, 363–387, https://doi.org/10.5194/essd-9-363-2017, 2017a.

Köhler, P., Nehrbass-Ahles, C., Schmitt, J., Stocker, T. F., and Fischer, H.: Continuous record of the atmospheric greenhouse gas carbon dioxide (CO2), final spline-smoothed data of calculated radiative forcing (Version 2), https://doi.org/10.1594/PANGAEA.876013, 2017b.

Lamy, F., Kilian, R., Arz, H. W., Francois, J.-P., Kaiser, J., Prange, M., and Steinke, T.: Holocene changes in the position and intensity of the southern westerly wind belt, Nat. Geosci., 3, 695–699, https://doi.org/10.1038/ngeo959, 2010.

Lehner, B. and Grill, G.: Global river hydrography and network routing: baseline data and new approaches to study the world's large river systems, Hydrol. Process., 27, 2171–2186, https://doi.org/10.1002/hyp.9740, 2013.

Lehner, B., Verdin, K., and Jarvis, A.: HydroSHEDS technical documentation, World Wildl. Fund US Wash. DC, 5, 2006.

Maldonado, A. and Villagrán, C.: Paleoenvironmental Changes in the Semiarid Coast of Chile (∼32°S) during the Last 6200 cal Years Inferred from a Swamp–Forest Pollen Record, Quat. Res., 58, 130–138, https://doi.org/10.1006/qres.2002.2353, 2002.

Maldonado, A. and Villagrán, C.: Climate variability over the last 9900 cal yr BP from a swamp forest pollen record along the semiarid coast of Chile, Quat. Res., 66, 246–258, https://doi.org/10.1016/j.yqres.2006.04.003, 2006.

Montade, V., Combourieu Nebout, N., Kissel, C., Haberle, S. G., Siani, G., and Michel, E.: Vegetation and climate changes during the last 22,000yr from a marine core near Taitao Peninsula, southern Chile, Palaeogeogr. Palaeoclimatol. Palaeoecol., 369, 335–348, https://doi.org/10.1016/j.palaeo.2012.11.001, 2013.

Moreno, P. I.: Millennial-scale climate variability in northwest Patagonia over the last 15 000 yr, J. Quat. Sci., 19, 35–47, https://doi.org/10.1002/jqs.813, 2004.

Moreno, P. I. and León, A. L.: Abrupt vegetation changes during the last glacial to Holocene transition in mid-latitude South America, J. Quat. Sci., 18, 787–800, https://doi.org/10.1002/jqs.801, 2003.

Moreno, P. I. and Videla, J.: Centennial and millennial-scale hydroclimate changes in northwestern Patagonia since 16,000 yr BP, Quat. Sci. Rev., 149, 326–337, https://doi.org/10.1016/j.quascirev.2016.08.008, 2016.

Moreno, P. I., Francois, J. P., Moy, C. M., and Villa-Martínez, R.: Covariability of the Southern Westerlies and atmospheric CO2 during the Holocene, Geology, 38, 727–730, https://doi.org/10.1130/G30962.1, 2010.

Moreno, P. I., Videla, J., Valero-Garcés, B., Alloway, B. V., and Heusser, L. E.: A continuous record of vegetation, fire-regime and climatic changes in northwestern Patagonia spanning the last 25,000 years, Quat. Sci. Rev., 198, 15–36, https://doi.org/10.1016/j.quascirev.2018.08.013, 2018.

Muñoz, P., Rebolledo, L., Dezileau, L., Maldonado, A., Mayr, C., Cárdenas, P., Lange, C. B., Lalangui, K., Sanchez, G., Salamanca, M., Araya, K., Jara, I., Easton, G., and Ramos, M.: Reconstructing past variations in environmental conditions and paleoproductivity over the last ∼ 8000 years off north-central Chile (30° S), Biogeosciences, 17, 5763–5785, https://doi.org/10.5194/bg-17-5763-2020, 2020.

Muratli, J. M., Chase, Z., McManus, J., and Mix, A.: Ice-sheet control of continental erosion in central and southern Chile (36°–41°S) over the last 30,000 years, Quat. Sci. Rev., 29, 3230–3239, https://doi.org/10.1016/j.quascirev.2010.06.037, 2010.

Ortega, C., Vargas, G., Rutllant, J. A., Jackson, D., and Méndez, C.: Major hydrological regime change along the semiarid western coast of South America during the early Holocene, Quat. Res., 78, 513–527, https://doi.org/10.1016/j.yqres.2012.08.002, 2012.

Perren, B. B., Kaiser, J., Arz, H. W., Dellwig, O., Hodgson, D. A., and Lamy, F.: Poleward displacement of the Southern Hemisphere Westerlies in response to Early Holocene warming, Commun. Earth Environ., 6, 1–10, https://doi.org/10.1038/s43247-025-02129-z, 2025.

Pesce, O. H. and Moreno, P. I.: Vegetation, fire and climate change in central-east Isla Grande de Chiloé (43°S) since the Last Glacial Maximum, northwestern Patagonia, Quat. Sci. Rev., 90, 143–157, https://doi.org/10.1016/j.quascirev.2014.02.021, 2014.

Pöppelmeier, F., Jeltsch-Thömmes, A., Lippold, J., Joos, F., and Stocker, T. F.: Multi-proxy constraints on Atlantic circulation dynamics since the last ice age, Nat. Geosci., 16, 349–356, https://doi.org/10.1038/s41561-023-01140-3, 2023.

Shakun, J. D., Clark, P. U., He, F., Marcott, S. A., Mix, A. C., Liu, Z., Otto-Bliesner, B., Schmittner, A., and Bard, E.: Global warming preceded by increasing carbon dioxide concentrations during the last deglaciation, Nature, 484, 49–54, https://doi.org/10.1038/nature10915, 2012.

Stuut, J.-B. W. and Lamy, F.: Climate variability at the southern boundaries of the Namib (southwestern Africa) and Atacama (northern Chile) coastal deserts during the last 120,000 yr, Quat. Res., 62, 301–309, https://doi.org/10.1016/j.yqres.2004.08.001, 2004.

Valero-Garcés, B. L., Jenny, B., Rondanelli, M., Delgado-Huertas, A., Burns, S. J., Veit, H., and Moreno, A.: Palaeohydrology of Laguna de Tagua Tagua (34° 30′ S) and moisture fluctuations in Central Chile for the last 46 000 yr, J. Quat. Sci., 20, 625–641, https://doi.org/10.1002/jqs.988, 2005.

Vargas-Ramirez, L., Roche, E., Gerrienne, P., and Hooghiemstra, H.: A pollen-based record of late glacial–Holocene climatic variability in the southern lake district, Chile, J. Paleolimnol., 39, 197–217, https://doi.org/10.1007/s10933-007-9115-0, 2008.

Villa-Martínez, R., Villagrán, C., and Jenny, B.: The last 7500 cal yr B.P. of westerly rainfall in Central Chile inferred from a high-resolution pollen record from Laguna Aculeo (34°S), Quat. Res., 60, 284–293, https://doi.org/10.1016/j.yqres.2003.07.007, 2003.

Waterisotopes Database: Global precipitation, 2017.